Emerin deficiency drives MCF7 cells to an invasive phenotype

Emily Hansen[1,2], Matthew Wang [1,3], Christal Rolling [1,2], James M. Holaska* [1,2]

[1]Department of Biomedical Sciences, Cooper Medical School of Rowan University, Camden, NJ, [2]Molecular and Cell Biology and Neuroscience Program, Rowan-Virtua School of Translational Biomedical Engineering and Sciences, Stratford, NJ, [3]Rowan-Virtua School of Osteopathic Medicine

*To whom correspondence should be addressed:
James M. Holaska
Cooper Medical School of Rowan University
Department of Biomedical Sciences, MEB 534
401 South Broadway
Camden, NJ. 08103
856-956-2746
holaska@rowan.edu

Keywords: Emerin, nucleoskeleton, metastasis, breast cancer

Word Count:

Figures and Tables:

Conflicts of Interest:

Authors have no conflicts of interest to disclose.

Acknowledgements:

We thank the Department of Biomedical Sciences at Cooper Medical School of Rowan University for providing funding for this work and many fruitful discussions. We thank Dr. Isabelle Mercier (St. Joseph's University) for many fruitful discussions regarding these studies. We thank the members of Holaska's lab for the numerous discussions

pertaining to this manuscript and the Boehning lab (Cooper Medical School at Rowan University) for technical help as needed during experiments.

Author Contributions:

J.H. and E.H. conceived the project. E.H., M.W., and C.R. created the cell lines together. E.H. and M.W. performed the trans-well and nuclear area experiments and analyzed the data. E.H. performed and analyzed the nuclear volume measurements. M.W. and C.R. performed the proliferation studies. E.H. performed the IHC experiments and E.H. and J.H. analyzed the data in the IHC experiments. E.H. and J.H. contributed to the writing of the manuscript and all authors contributed input in figure preparation and in writing of the manuscript.

Funding:

This work was supported by a grant from the National Institute of Arthritis, and Musculoskeletal and Skin Diseases (R15AR069935 to JH) and a grant from the New Jersey Commission on Cancer Research (COCR22RBG007 to JH). The content is solely the responsibility of the authors and does not necessarily represent the official views of the National Institutes of Health or the New Jersey Commission on Cancer Research. This work was also supported by Rowan University under the Camden Health Research Initiative.

Competing Interests:

The authors declare no competing interests.

Abstract: (1074 Characters, 150 words)

During metastasis, cancer cells traverse the vasculature by squeezing through very small gaps in the endothelium. Thus, nuclei in metastatic cancer cells must become more malleable to move through these gaps. Our lab showed invasive breast cancer cells have 50% less emerin protein resulting in smaller, misshapen nuclei, and higher metastasis rates than non-cancerous controls. Thus, emerin deficiency was predicted to cause increased nuclear compliance, cell migration, and metastasis. We tested this hypothesis by downregulating emerin in noninvasive MCF7 cells and found emerin knockdown causes smaller, dysmorphic nuclei, resulting in increased impeded cell migration. Emerin reduction in invasive breast cancer cells showed similar results. Supporting the clinical relevance of emerin reduction in cancer progression, our analysis of 192 breast cancer patient samples showed emerin expression inversely correlates with cancer invasiveness. We conclude emerin loss is an important driver of invasive transformation and has utility as a biomarker for tumor progression.

Introduction

Nuclear morphology is well-established as an effective diagnostic tool in grading many cancers.[1] Changes in nuclear morphology and nuclear compliance (i.e., nuclear softening) is associated with tumor aggressiveness and metastasis,[2-4] and is recognized as a 'hallmark of cancer.'[5, 6] Breast cancer metastasis is responsible for a majority of breast cancer-related deaths, making it a significant clinical concern.[6] For cancer to metastasize, cancerous tumor cells must first invade the extracellular matrix and then enter the vasculature by squeezing through small gaps in the vascular endothelium. To establish a metastatic tumor, these cells travel through the body and exit the vasculature by squeezing through these gaps in the endothelium to create satellite tumors.[6] These gaps in the endothelium are relatively small, ranging from 1.2-2 microns in diameter.[7] Although the cytoplasm of cells may fit through gaps of this size, the nucleus serves as a physical barrier because it has a diameter of about 10-20 microns and a stiffness more than twice that of the cytoplasm.[8]

Nuclear stiffness is governed by a complex set of nucleostructural proteins that serve as signaling molecules and scaffolds. For example, emerin, an inner nuclear membrane protein that binds to lamins, is also responsible for regulating nuclear structure.[9-11] Interestingly, emerin is reported to be mutated in cancers, specifically in its nucleoskeletal binding domain.[10] We previously showed that triple-negative breast cancer (TNBC) cell lines have significantly less emerin expression than their non-cancerous controls.[11] This decreased emerin expression correlated with decreased nuclear size and increased migration and invasion.[11] Expressing GFP-emerin rescued

these deficits, while GFP-emerin mutants that failed to bind nuclear actin and lamins were unable to rescue nuclear size, migration, or invasion.[11] In mice, we found that expressing wildtype GFP-emerin in MDA-231 cells decreased primary tumor size and lung metastasis compared to MDA-231 cells expressing GFP.[11] GFP-emerin mutants that blocked binding to nuclear actin or lamins failed to inhibit tumor growth and metastasis in MDA-231 cells, demonstrating that emerin's function in metastatic spread is likely dependent on its role in regulating the nucleoskeleton.[11] Emerin expression also inhibits metastasis in prostate cancer,[12] supporting emerin's involvement in metastatic disease.

While these findings show that emerin has a role in metastatic disease via its nucleoskeletal interactions, they fail to ascertain whether reduced emerin protein expression is sufficient to reduce nuclear structure and increase cell migration and invasion, or if the reduced emerin expression was a result of the invasive transformation of MDA-231 cells. Thus, we tested if downregulating emerin in non-invasive cells is sufficient to convert them to a more invasive phenotype, similar to that of MDA-231 cells. Here, we show that knocking-down emerin in poorly invasive MCF7 cells does promote migration and is accompanied by smaller, more deformed nuclei, suggesting a critical link between emerin protein reduction and metastatic properties of cancer cells.

Results

To examine the effect of emerin downregulation on MCF7, we generated MCF7 cell lines expressing either one of three different emerin shRNA sequences (A, B, C) or a scrambled shRNA sequence (Genecopoeia). We found emerin shRNA A reduced

emerin protein by 80%, emerin shRNA B failed to reduce emerin expression, and emerin shRNA C reduced emerin protein expression by 55% (**Figure 1**). Emerin shRNA sequence B serves as our control (now named con shRNA) because it failed to reduce emerin protein expression. Thus, unless otherwise noted, the experiments using MCF7 cells were done using emerin shRNA B as the control (con shRNA), and emerin shRNA A (emerin shRNA).

Reduction of emerin protein expression by 80% (**Figure 2A**) caused MCF7 cells to reduce nuclear size by 14% (**Figure 2B,C**), as measured using the ImageJ ParticleAnalyzer plug-in (see methods). It was possible that decreased nuclear area was caused by rounding of the nuclei, without a change in nuclear size. Thus, nuclear volume was measured in 25 or more nuclei per cell line. Nuclei from MCF7 and con shRNA cell lines were 528.9 ± 16.7 μm^3 and 478.4 ± 18.49 μm^3, respectively (**Figure 3A,B**). Emerin knockdown reduced nuclear volume to 369.1 ± 15.62 μm^3 (**Figure 3A,B**,) showing emerin deficiency reduced nuclear size. To test whether nuclear structure itself was being altered, we also generated 3D renderings of nuclei from each cell line and measured nuclear curvature. To analyze local membrane curvature of nuclei, we used the LimeSeg plugin for Fiji.[13] Using LimeSeg, we created three dimensional renders of the nuclei and then calculated the gaussian and mean curvature at 0.5 nm intervals across the surface. From this, we calculated the fraction of points that had both a positive gaussian curvature and negative mean curvature, which indicates a “concave” surface. We found significantly more indentations and bulges in the emerin shRNA lines (**Figure 3C**). Thus, nuclei in the emerin-deficient MCF7 cells were smaller and more dysmorphic than controls.

Trans-well migration assays were done to test if these nuclear changes in emerin-downregulated MCF7 cells increased impeded migration. Emerin-downregulated MCF7 cells increased migration through 8 µm trans-well pores by 3.2-fold and 2.82-fold when compared to MCF7 and con shRNA cells, respectively (**Figure 4A,B**). To separate the nuclear structural aspects of impeded migration from the more generalized signaling and cytoskeleton reorganization associated with responding to migratory cues, we tested unimpeded migration in scratch-wound assays. Interestingly, emerin shRNA cells migrated into the scratch-wound 10% faster than MCF7 or con shRNA cells (**Figure 4C,D**).

We then tested whether triple-negative breast cancer cells, which already express 50% less emerin compared to normal breast cells[11] and are highly invasive, would become more invasive when emerin protein expression is reduced further. We transfected our MDA-231 cells with the same emerin shRNA plasmids as the MCF7 cells above. We found MDA-231 emerin shRNA lines did reduce emerin further by 59% (**Figure 5B**). However, neither nuclear area (**Figure 5C)** nor nuclear volume (**Figure 6A-B)** decreased in emerin shRNA cell lines. Despite there being no change in nuclear area or volume, there was a significant increase in nuclear concavity with many of the emerin shRNA nuclei being highly deformed (**Figure 6A,C).** This increased nuclear deformation coincided with increased migration of emerin shRNA MDA-231 cells through 8-micron trans-well pores compared to the control (**Figure 7A-B**). Downregulation of emerin had no effect on unimpeded migration (**Figure 7C-D**).

Because emerin was implicated in regulating proliferation of MDA-231 cells,[11] we examined cell proliferation in MCF7 cells, emerin-downregulated MCF7 cells and con shRNA MCF7 cells to test if emerin deficiency increased MCF7 proliferation. Emerin downregulation increased cell proliferation in two different assays There was a 1.4-fold increase in cell proliferation by day 7 in emerin shRNA MCF7 cells compared to the con shRNA MCF7 cells by cell counting (**Figure 8A)** and a 1.3-fold increase in proliferation by day 6 in the Presto-Blue assay (**Figure 8B**). This assay produced similar results in MDA-231 cells, where there was a 2.5 increase in proliferation by day 6 when measured via the Presto-Blue assay **(Figure 8C).** It is important to note that these assays do have approximately a two-day lag time in growth before seeing such affects, which is consistent with other published cell cycle data.[14, 15]

These data strongly suggest that loss of emerin drives invasive cancer progression. Further, we previously found that emerin protein expression was decreased in a small sample of breast cancer patients.[11] To rigorously determine if emerin protein expression inversely correlates with cancer invasiveness in patients, we analyzed emerin expression on 216 patient samples by immunohistochemistry with emerin antibodies (10351-1-AP, Proteintech) on a tissue microarray (TissueArray, LLC). This array contained breast cancer tumor samples from a range of types and grades. Each tumor was graded for emerin expression at the nuclear envelope based on the amount of emerin staining at the nuclear periphery; this accounts for both protein expression and normal localization.[10] The grader was blinded to sample identifiers. We found emerin expression at the nuclear envelope is lower in metastatic tissue, ductal carcinoma in-situ tissue, and malignant tissue, while normal, adjacent-to-cancer normal, or benign

tumor tissue had normal emerin expression at the nuclear envelope (**Figure 9**). To validate these results, we used a different emerin antibody from a different species (cat# 6096097, Leica) to stain an identical tissue microarray, which gave similar results (**Figure 10)**. Note that similar to the results with the emerin polyclonal antibody, emerin nuclear envelope levels were trending lower in DCIS, but more samples are needed to increase statistical power. To confirm that these results were emerin-specific, we stained this tissue microarray with just secondary antibody to account for background staining (**Figure S2**).

Discussion

It has been established for decades that the presence of abnormal nuclear structure could help distinguish tumor cells from normal cells, and to grade tumors.[16] Yet, the contribution of these nuclear alterations to malignant transformation is unclear. Here, we show that downregulating emerin in non-invasive MCF7 cells was sufficient to decrease nuclear size, to increase nuclear deformation, and to increase impeded cell migration. Such qualities are indicative of invasive cancers.[10, 17] Importantly, these phenotypes were not due to the presence of the shRNA vector or cell line selection conditions because the scrambled shRNA and con shRNA had similar phenotypes as MCF7 cells. Thus, we conclude that loss of emerin is crucial for transforming benign tumor cells to a more invasive phenotype. Consistent with our results, reduction in emerin also correlated with nuclear softening in melanoma cells,[18] something that is well-established to correlate with rates of invasiveness and metastasis.[19, 20] Interestingly, emerin shRNA cells migrated into the scratch-wound 10% faster than MCF7 or con shRNA cells

(**Figure 4C,D**). We suspect this is caused by a disruption in mechanical signaling, as multiple labs have shown that disrupting the linker of nucleoskeleton and cytoskeleton (LINC) complex impairs cells' ability to close scratch wounds.[14, 21, 22]

Knocking down emerin in MDA-231 cells did not affect nuclear area. MDA-231 cells are highly invasive TNBCs that also have 50% less emerin than normal primary breast epithelial cells, MCF10A cells,[11] and MCF7 cells (**Figure S1**). We propose that the MDA-231 nucleus is already at is minimal size, given nucleoplasmic, chromatin, and nuclear membrane constraints, so further reduction of emerin has no effect on nuclear size. Rather emerin reduction increases the compliance of the nucleus to make it more malleable.

Consistent with these results showing emerin-deficiency drives cancer cell invasiveness, our blinded analysis of 216 breast cancer patient samples showed that lower emerin levels correlated with increased aggressiveness. These results support a model by which emerin downregulation occurs in a cell population within a growing tumor. These cells would then be selected during tumor evolution because of their increased proliferation and increased nuclear compliance, which allows them to be more invasive. This increased invasiveness enables the cells to invade the extracellular matrix and squeeze through the vascular endothelium to promote increased cancer cell survival and metastasis. Supporting our results, recent studies in prostate[12] and ovarian cancer,[23] found that patients have decreased emerin and that this decreased emerin contributes to higher nuclear deformity and invasion.[12]

We are aware that emerin levels do not always inversely correlate with nuclear size across all cell types.[20, 24] However, increased nuclear deformation and increased compliance in emerin-deficient cells seem to be shared across many cell types.[24] Whether the cell-type specificity of emerin reduction in nuclear size are caused by differences in cytoskeletal forces pushing more (to induce smaller nuclei) or less (to allow for nuclear expansion) on the nuclei, or on limiting amounts of nuclear envelope lipid components, nuclear pore complex proteins, or other nuclear envelope proteins, remains to be determined..

Collectively, these data demonstrate that emerin is critical for maintaining nuclear structure and rigidity, the loss of which makes nuclei more compliant. Based on our data, we suggest a model by which emerin expression is necessary for maintaining nuclear structure under cellular stress. Therefore, loss of emerin, such as in cancer, contributes to increased nuclear compliance, further driving tumor cell aggressiveness, invasiveness, and metastatic transformation (**Figure 11**). By further investigating emerin's role in breast cancer progression, targetable treatments for even the most invasive breast cancer types, such as triple-negative breast cancer, may be revealed.

Materials and methods

Cell Culture

MDA-MB-231 (ATCC cat#: HTB-26) and MCF10A (ATCC cat#: CRL-10317) were purchased from American Type Culture Collection (ATCC, Manassas, VA). MCF7 cells (ATCC cat#: HTB-22) were obtained from Mary Alpaugh's lab (Rowan University,

Camden NJ). The MDA-231 and MCF7 cells were grown in Dulbecco's Modified Eagle Medium + GlutaMAX (Gibco cat#:10566024) with 10% Fetal Bovine Serum (Gibco, cat#: 16140089) and 1% Penicillin/Streptomycin. MCF10A cells were grown in Ham's F-12 (Modified) + L-glutamine media (Corning, Cat#: 10-080-CV) with 5% horse serum (Gibco/Life Technologies, cat#: 16050–130), 0.5 mg/ml hydrocortisone (ThermoFisher Scientific, Waltham, MA, cat#: AC35245–0010), 100 ng/ml cholera toxin (MilliporeSigma, Burlington, MA, cat#: 227036), 10 µg/ml Insulin (Sigma-Aldrich, St. Louis, MO, cat#: 10516), and 1% Penicillin/Streptomycin. All cells were grown at 37^{o}C and 5% CO_2. Mycoplasma testing is done bimonthly using the MycoStrip 100 kit (InvivoGen, cat#: rep-mysnc-100).

Creating Stable Cell Lines

Cell lines were transfected via the Neon Electroporation System (Invitrogen) or with Lipofectamine 3000 (cat# L3000015, Invitrogen). For electroporation, cells were resuspended in buffer "R" provided with the Neon Kit per manufacturer instructions. Electroporation was done using 1400 V for 10 ms for 4 pulses with the 100 µl tips. Cells were plated in their respective media without penicillin/streptomycin for 24 hours before being replaced with full media. For Lipofectamine 3000 transfection, cells were seeded in a 6-well plate at 70% confluency and transfected with 5 µl of Lipofectamine 3000 per reaction. Plasmids were introduced at 2 ng/µl of each (emerin shRNA, HSH095287-LVRU6MH; shRNA scramble sequence, CSHCTR001-LVRU6MH; Genecopoeia). For both methods, cells expressing the various shRNAs were selected with 0.2 mg/ml

hygromycin (cat#K547-20ml, VWR) at 72-hours post transfection and maintained at 0.8 mg/ml of hygromycin after cell line purification.

Immunofluorescence, volume, and nuclear area measurement

Cell lines were plated on coverslips at approximately 100,000 cells/coverslip and placed in 6-well plates. Cells were rinsed three times with 2 ml of PBS for 5 minutes and fixed with 3.7% formaldehyde in PBS for 15 minutes. Coverslips were washed again three times and permeabilized in 2 ml of 0.2% Triton X-100 in PBS for 24 minutes. Cells were blocked for 1 hour in 2 ml of 3% BSA in PBS (VWR, cat#: 97063-624). Cells were then washed three times with 2 ml of PBS for 5 minutes each and mounted with Prolong Diamond Antifade Mountant (Molecular Probes, cat#: P36971). Slides were imaged using either the Evos FL Auto Microscope using a 40x objective or Nikon confocal with 100x objective. Nuclear area was measured via Image J ParticleAnalyzer plugin. Briefly, images were transformed into a binary image where ParticleAnalyzer could then measure each nucleus. Nuclei on the edges of the image or touching other nuclei were excluded. Nuclear volume was measured via ImageJ FIJI 3D Objects Counter Plugin following the same parameters. Statistical significance was determined via one-way ANOVA followed by Dunnett's multiple comparison test, where applicable.

Concavity Measurements

Concavity was measured via the LimeSeg plugin for Fiji as outlined in Machado et. al.[13] Using the plugin's "sphere seg" command, we created three dimensional renders of the nuclei taken at 100x in a z-stack (Nikon) with 0.5-micron steps. Then, using the

"ComputeCurvatures" and "DisplayCurvatures" scripts in the plugin, we calculated the mean curvature at each point along the surface at 0.5 nm intervals, and displayed regions of positive mean curvature in green and regions of negative mean curvature in red. Statistical significance was determined via one-way ANOVA followed by Dunnett's multiple comparison test, where applicable. A minimum of 15 nuclei were rendered and measured.

Trans-well Migration Assays

Trans-well inserts with 8-micron pores (Falcon, Cat#: 353097) were used for cell migration. Cells were plated in the chamber at a density of 1.5 x10^5 in serum-free media. Chambers were placed in 24-well plates containing complete growth media. After 24 hours, cells that failed to migrate through the trans-well were wiped off the top of the membrane and the cells on the bottom of the membrane were fixed for 15 minutes with 3.7% formaldehyde in PBS. The membranes were then washed 3 times in 750 µl of PBS for 5 minutes and treated with 750 µl of 0.5% Triton X-100 for 20 minutes to permeabilize membranes. The membranes were then washed a final three times with PBS and removed and mounted, cell-side down, with Prolong Diamond Antifade Mountant (Molecular Probes, cat#: P36971). Cells that migrated through were counted (five fields on the Evos FL Auto Microscope, 40x objective) after allowing the mountant to dry overnight. Statistical significance was determined via one-way ANOVA followed by Dunnett's multiple comparison test, where applicable. At least three biological replicates were done for each cell type.

Scratch Wound Assays

Each of the MCF7 and MDA-231 cell lines was grown to confluency in 12-well plates. A 1 mm scratch was made in each well. Plates were marked to ensure images were taken at the same location at each timepoint. Images were taken until the wound closed entirely on the Evos FL Auto Microscope using the 40x objective. Statistical significance was determined via one-way ANOVA. 3 biological replicates were done for each cell line.

Cell Proliferation Assays

For the cell counting method, each cell line was seeded at 20,000 cells per well of a 6-well dish (total of 7 wells). Each day for 7 days, one well was trypsinized and counted on the Countess II FL (Life Technologies). Two-way ANOVA was completed to determine statistical significance followed by Tukey's test where applicable. Two-way ANOVA was completed with Tukey's test for significance. Both experiments include three biological replicates.

The parallel cell proliferation analysis was completed using the PrestoBlue Cell Viability reagent (Life Technologies, cat#: A13261) per manufacturer's instructions. Proliferation was analyzed by plating 2 x 10^4 cells of each cell line in a 96-well plate and cell growth was monitored every 24 hours for 7 days after plating. At least three biological replicates were done for each cell line.

Western Blots

Whole cell lysates were suspended in NuPAGE LDS Buffer (LifeTechnologies, cat#: NP0008) with reducing agent (LifeTechnologies, cat#: NP0009). Samples were resolved by 10% SDS-PAGE gels (materials from Bio-Rad) and transferred to nitrocellulose membranes (GE Healthcare, Cat#: 10600004). Membranes were blocked in 5% nonfat dry milk (Giant brand) in PBST for two hours. Primary emerin (Protein-tech, cat# 10351-1-AP, 1:3,000 dilution) and γ-tubulin (Sigma, cat# T6557, 1:25,000 dilution) antibodies were incubated overnight with rocking at 4°C and secondary antibodies (goat anti-rabbit [cat# 31462, Invitrogen, 1:10,000] or goat anti-mouse [cat#31432, Invitrogen, 1:10,000] IgG H&L cross absorbed HRP) were incubated for 2 hours at room temperature. Emerin protein expression was normalized to γ-tubulin protein expression for quantification. Western blots were imaged on the Li-COR Odyssey FC. Statistical significance was determined via one-way ANOVA.

Immunohistochemistry and Tissue Microarray Analysis

Tissue microarrays (TissueArray, LLC, cat# BR2082c) were deparaffinized and rehydrated in coplin jars (5 minutes in xylene three times, 3 minutes in 100% EtOH three times, 3 minutes in 95% EtOH three times, 3 minutes in 80% EtOH, 3 minutes in 70% EtOH, and 5 minutes in distilled water) prior to being placed in citrate buffer (0.05% Tween 20, 10mM citric acid at pH 6.0) and steamed at 95°C for 45 minutes. Slides were cooled at RT and washed with PBS. Endogenous peroxidase was removed by washing with 0.3% hydrogen peroxide for 20 minutes at room temperature in coplin jars. After washing again with PBS, slides were blocked in 1% Bovine Serum Albumin (VWR, cat#: 97061-420) in PBS for 15 minutes. Slides were then incubated with anti-emerin

antibody (Proteintech, cat#: 10351-1-AP, 1:500 dilution) for two hours at 37ºC in a humidified chamber. Slides were washed again with PBS and blocked with 2.5% Normal Goat Serum for 20 minutes at room temperature (ImmPRESS Reagent, Vector Lab, cat#: MP-7451) and then incubated with the anti-rabbit ImmPRESS IgG peroxidase reagent (Vector Lab, cat#: MP-7451) or the anti-mouse ImmPRESS IgG peroxidase reagent (Vector Lab, cat# MP-7452) per manufacturer instructions. Slides were washed again with PBS and incubated with the ImmPACT DAB peroxidase substrate (Vector Lab, cat#: SK4105) for 90 seconds at room temperature while checking color development under a microscope before rinsing in tap water. Slides were counterstained with Vector Hematoxylin (Gill's Formula, Vector Lab, cat#: H3401) for three minutes. After rinsing again in tap water, slides were incubated in 0.1% sodium bicarbonate for one minute, rinsed with distilled water, and then dehydrated and mounted with Prolong Diamond Antifade Mountant (Invitrogen, cat#: P36970). Tissue images were taken on the Evos FL Auto microscope and the Precipoint slide scanning microscope. Blinded grading of tissues was done using a grading system in which a 0 corresponded to no emerin staining at the nuclear periphery and a 3 being complete, dark staining of emerin at the nuclear periphery. All grading was done in one sitting to avoid multi-day bias. Invasive, DCIS, and metastatic tissue measurements were determined significant against noncancerous tissue *a priori* via student's t-test.

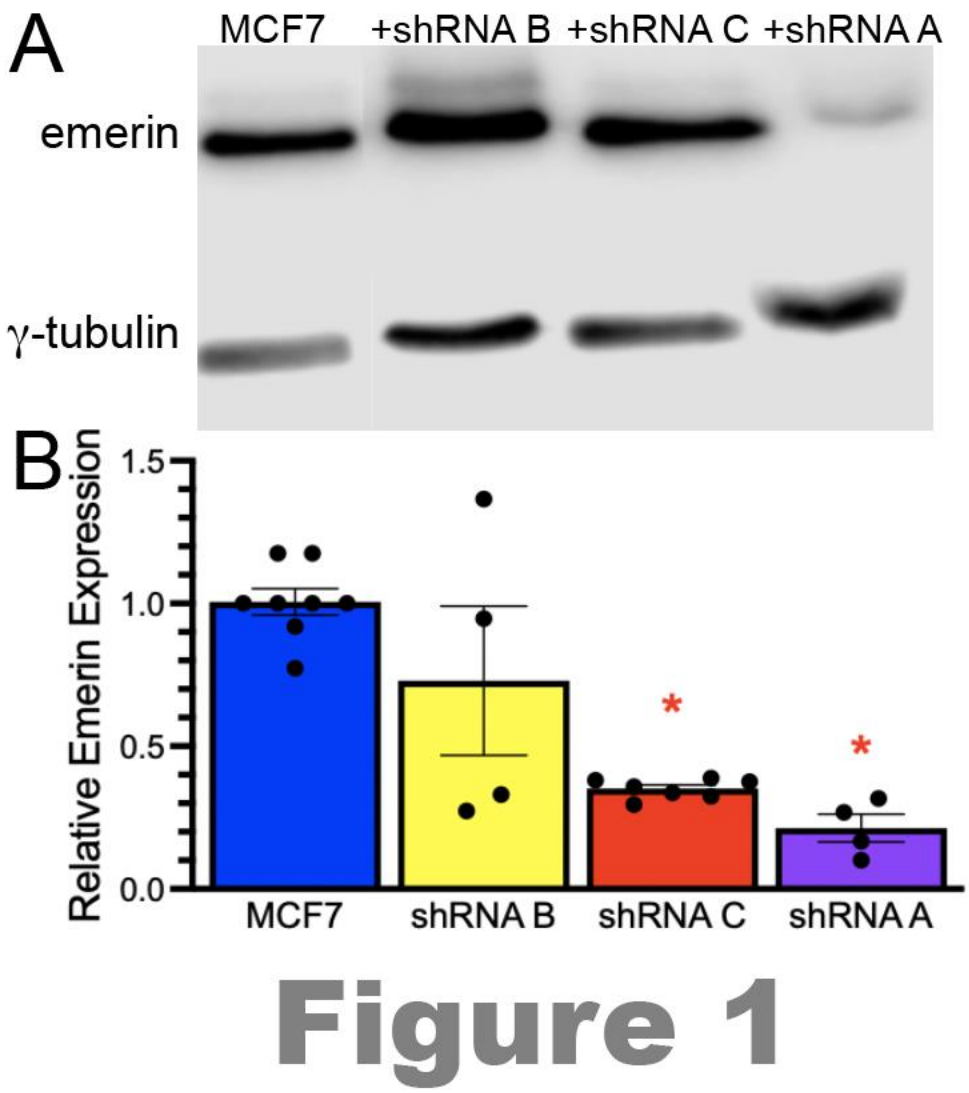

Figure 1

373 **Figure 1: Emerin protein expression in MCF7 and MCF7 emerin shRNA-**

374 **transfected cell lines.** A) Representative western blot and B) quantification of MCF7

375 and three emerin shRNA cell lines normalized to γ-tubulin. *P<0.001, N=6, one way

376 ANOVA followed by Dunnett's multiple comparison against MCF7.

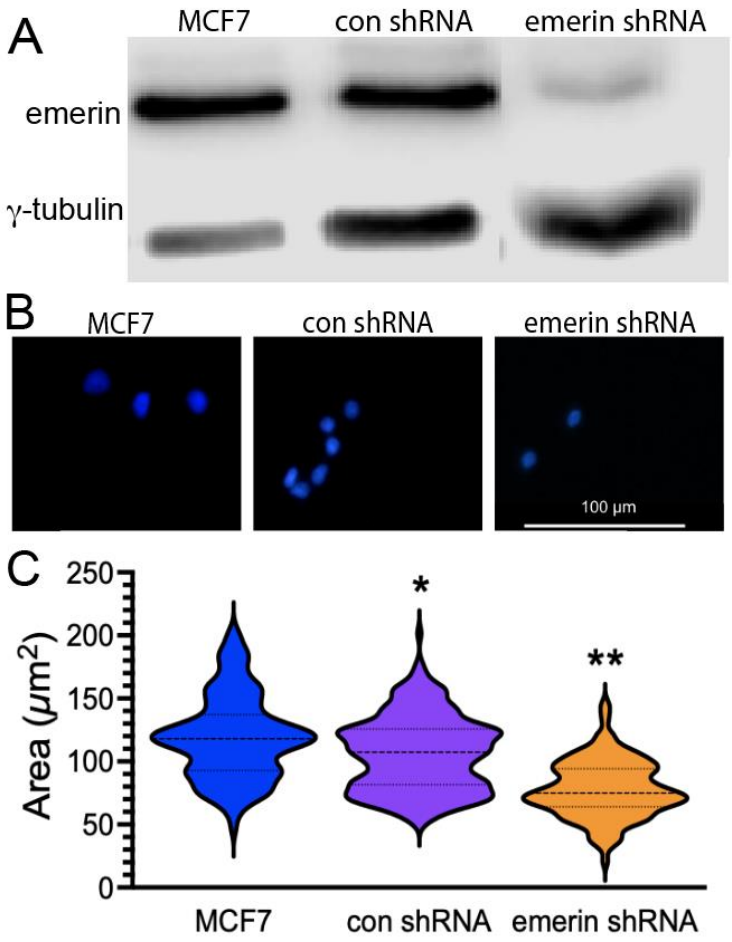

Figure 2

Figure 2: Reducing emerin in MCF7 cells decreased nuclear area. A) Representative western blots of MCF7, control shRNA, and emerin shRNA cell lines using emerin antibodies and γ-tubulin antibodies (loading control). B) Representative DAPI images of MCF7, control shRNA, and emerin shRNA cell lines, which were used to measure nuclear area. C) Violin plot of nuclear area of MCF7, control shRNA and emerin shRNA MCF7 cells (N>50 nuclei). The mean is depicted as the dark dashed line and the thin dashed lines represent the first and third quartiles. *P<0.001 **P<0.0001, one-way ANOVA followed by Dunnett's multiple comparison.

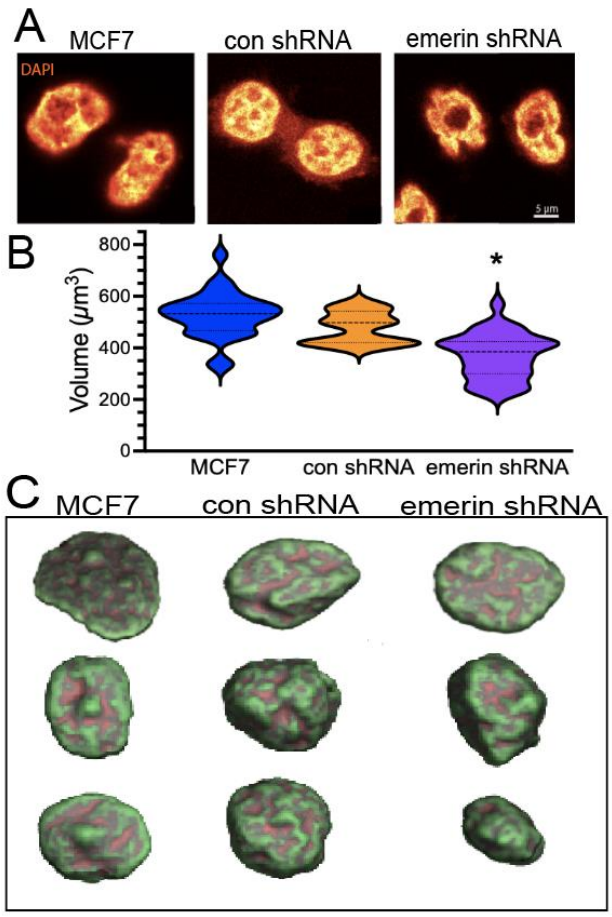

Figure 3

Figure 3: Emerin reduction decreases nuclear volume and increases nuclear bulges and indentations in MCF7 cells. A) Representative confocal images of DAPI-stained nuclei from MCF7, control shRNA, and emerin shRNA lines. B) Violin plots of nuclear volumes (N>15 nuclei for each) of MCF7, control shRNA, and emerin shRNA MCF7 cell lines. The mean is depicted as the dark dashed line and the thin dashed lines represent the first and third quartiles. *P<0.0001, one-way ANOVA followed by Dunnett's multiple comparison test. C) 3-D rendering of z-stacks from representative nuclei in B showing the concavity and convexity of the nuclei. Red-orange indicates a concave surface and green indicates a convex surface.

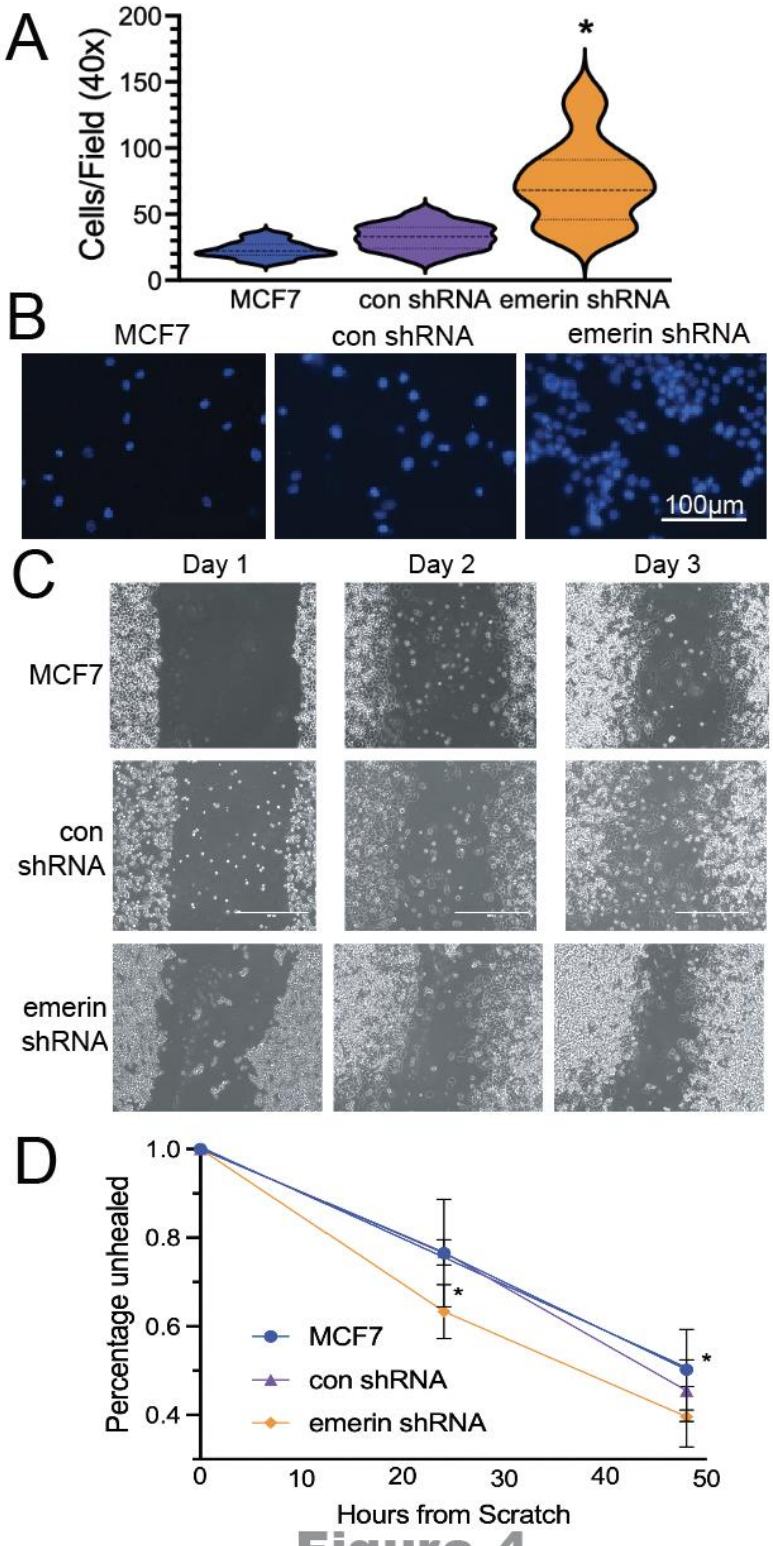

Figure 4

Figure 4: Reducing emerin in MCF7 cells increases impeded migration and closes scratch wounds faster. A) A violin plot of the number of cells migrating through 8 µm trans-well pores is shown for MCF7, control shRNA, and emerin shRNA cell lines (n=5 fields) The mean is depicted as the dark dashed line and the thin dashed lines represent the first and third quartiles. *P<0.0001, one-way ANOVA followed by Dunnett's multiple comparison. B) Representative DAPI images of the cells that successfully migrated in the trans-well assays in A. C) Scratch-wound healing assay. MCF7, control shRNA, and emerin shRNA MCF7 cell lines were plated, scratched with a pipette tip, and their migration into the wound area was monitored for 24, 48, and 72 hours. Representative phase images are shown. D) The rate of scratch wound healing, which refers to the ability of cells to migrate into the wound area is shown with standard deviation. *P<0.05 compared to MCF7, two-way ANOVA and Tukey's multiple comparison test.

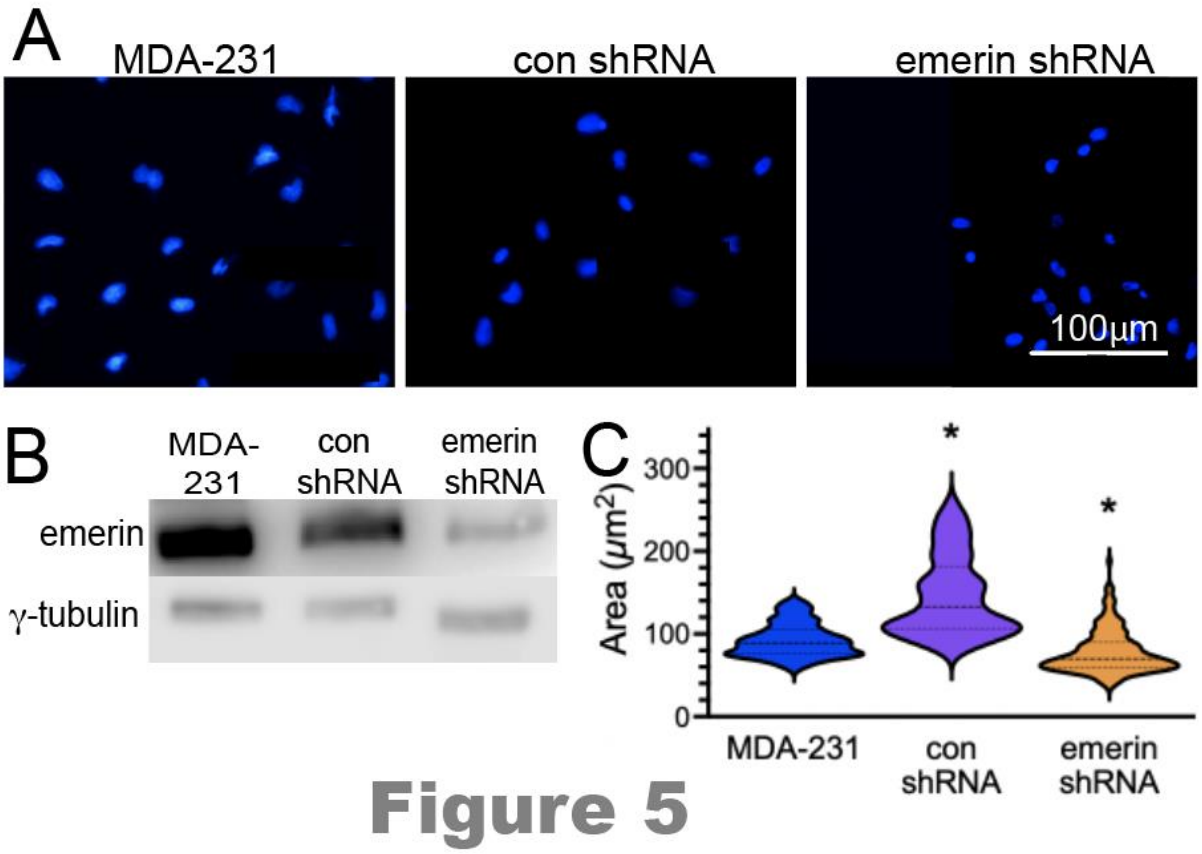

Figure 5

410

411 **Figure 5: Reducing emerin in MDA-231 lines fails to affect nuclear size.** A)
412 Representative images of nuclei in MDA-231, control shRNA, and emerin shRNA stable
413 cell lines that were used to measure nuclear area. B) Representative western blot of
414 emerin and γ-tubulin (loading control) in these lines. C) A violin plot of nuclear area of
415 MDA-231, control shRNA, and emerin shRNA MDA-231 cell lines. The mean is depicted
416 as the dark dashed line and the thin dashed lines represent the first and third quartiles
417 *P<0.0006, N>50 nuclei; one-way ANOVA followed by Dunnett's multiple comparison
418 test.

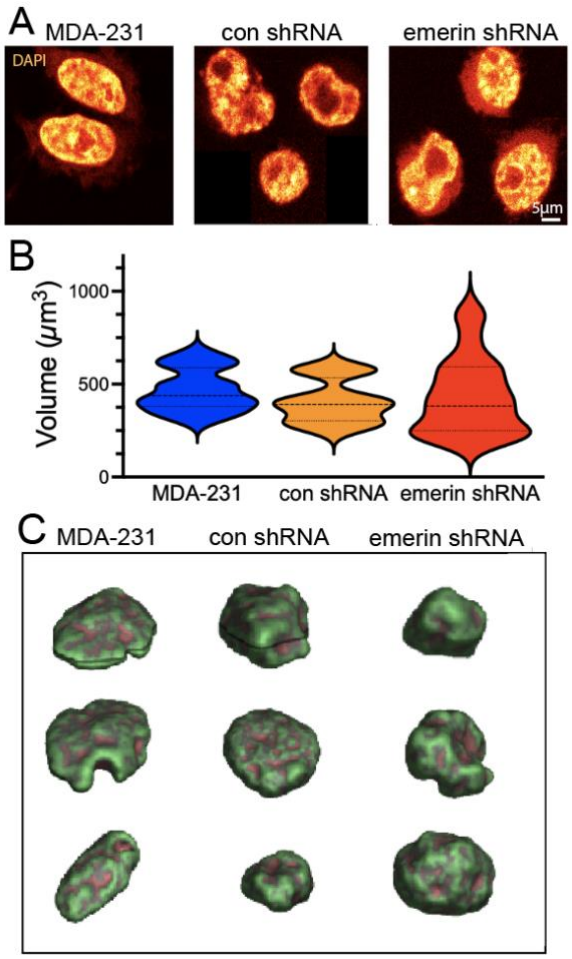

Figure 6

Figure 6: Reducing emerin in MDA-231 cells fails to decrease nuclear volume but increases nuclear deformations. A) Representative confocal images of DAPI-stained nuclei from MDA-231, control shRNA, and emerin shRNA MDA-231 cell lines. B) Violin plots of nuclear volumes (N>15 nuclei for each) of MDA-231, control shRNA, and emerin shRNA MDA-231 cell lines. The mean is depicted as the dark dashed line and the thin dashed lines represent the first and third quartiles. C) Representative images of convexity and concavity of nuclei in the respective cell lines. Red-orange indicates concave surface and green indicates a convex surface. No significant differences were seen using one-way ANOVA.

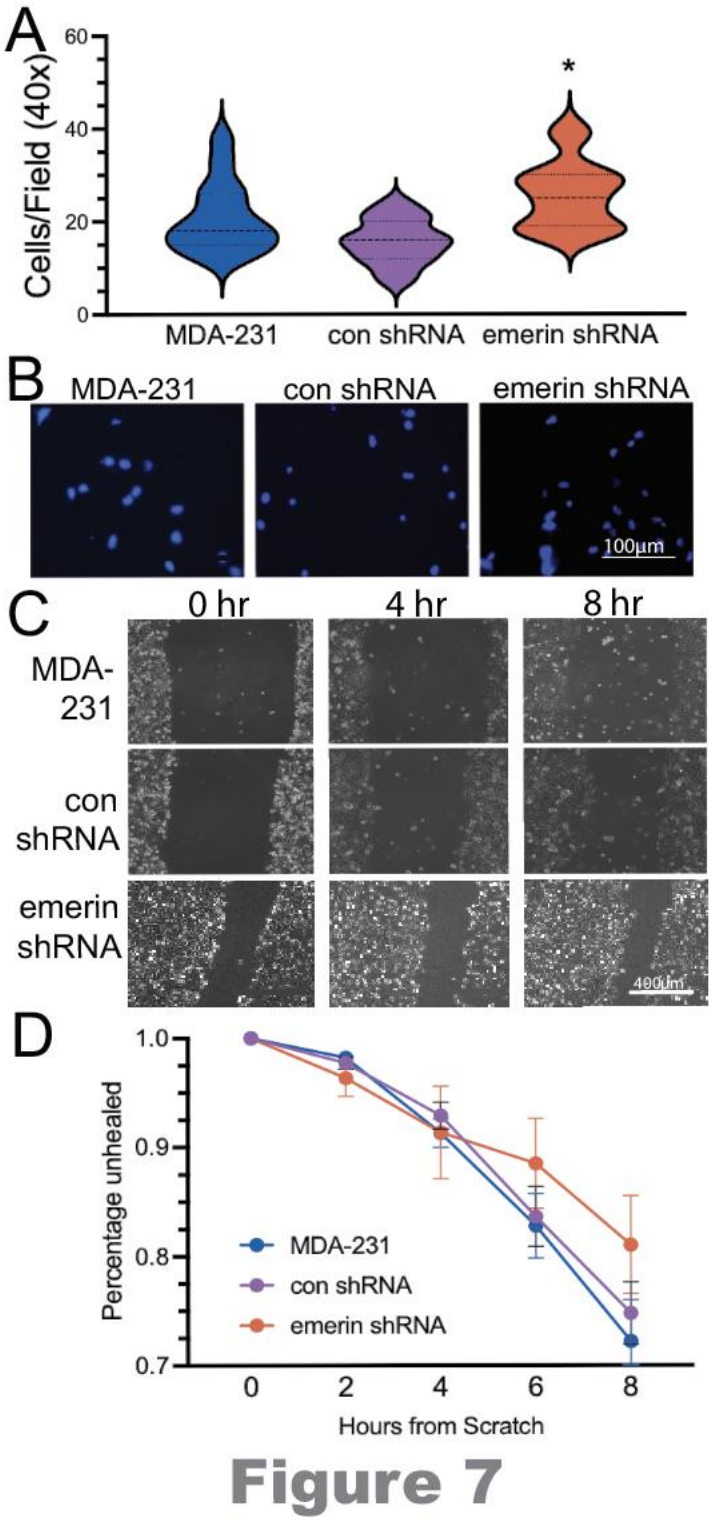

Figure 7

Figure 7: Reducing emerin in MDA-231 cells increases their impeded migration. A) A violin plot of the number of cells migrating through 8 µm trans-well pores is shown for

MDA-231, control shRNA, and emerin shRNA MDA-231 cell lines (n=5 fields) The mean is depicted as the dark dashed line and the thin dashed lines represent the first and third quartiles. *P<0.0037 compared to control shRNA, one-way ANOVA followed by Dunnett's multiple comparison; 3 biological replicates were used for each cell line. B) Representative DAPI images of the cells that successfully migrated in the trans-well assays in A. C) Scratch-wound healing assay. MDA-231, control shRNA, and emerin shRNA MDA-231 cell lines were plated, scratched with a pipette tip, and migration into the wound area was monitored every 2 hours for 8 hours. Representative phase images are shown. D) The rate of scratch wound healing, which refers to the ability of cells to migrate into the wound area, is shown with standard deviation. Two-way ANOVA was used, and no significant differences were seen.

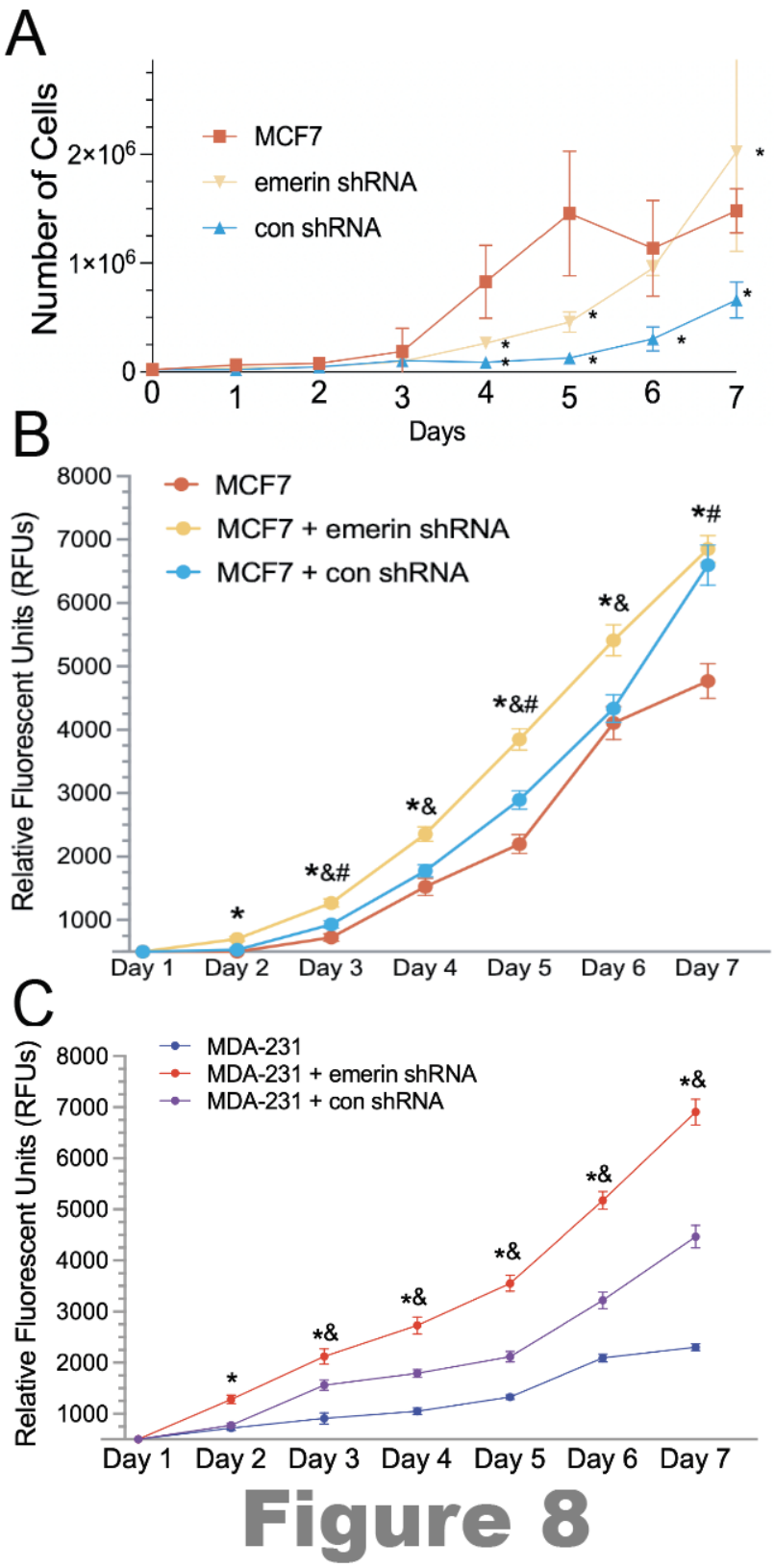

Figure 8

Figure 8: Reduction of emerin increases cell proliferation in MCF7 and MDA-231 cells. Growth curves of MCF7, emerin shRNA MCF7, and control shRNA MCF7 cells, as shown A) by cell counting and B) by measuring metabolic activity with Presto Blue Cell Viability Reagent (Life Technologies, cat#: A13261) per manufacturer's instructions. Mean data plotted with SEM; n = 3 biological replicates. * indicates a difference between MCF7 + emerin shRNA and MCF7 + control shRNA (*$p < 0.05$). & indicates a difference between MCF7 + emerin shRNA and MCF7 (& $p < 0.05$). # indicates a difference between MCF7 + control shRNA and MCF7 (# $p < 0.05$). C) Growth curves of MDA-231, emerin shRNA MDA-231, and control shRNA MDA-231 cells as determined using Presto Blue. Mean data plotted with SEM; n = 3 biological replicates. * indicates a significant difference between MDA-231 and MDA-231 + emerin shRNA (*$p < 0.05$), & indicates a significant difference between MDA-231, and MDA-231 + con shRNA (& $p < 0.05$), as determined by two-way ANOVA and Tukey's multiple comparison test.

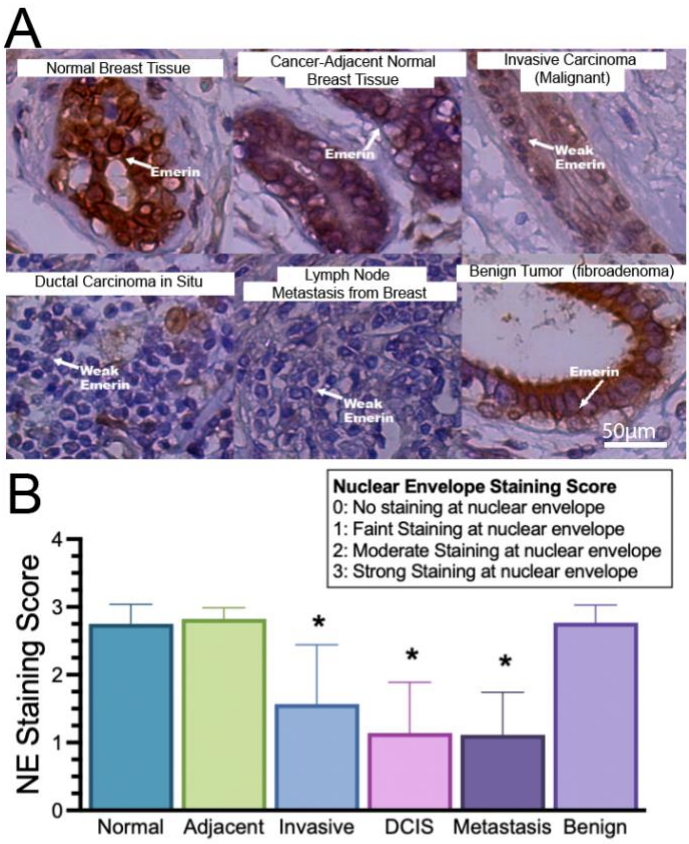

Figure 9

Figure 9: Reduced emerin expression at the nuclear periphery correlates with breast cancer invasiveness in patients. A) Representative tissue microarray staining of emerin in 183 patients using emerin polyclonal antibodies (Proteintech, cat# 10351-1-AP). Nuclei are blue, emerin is brown, and arrows denote emerin staining in certain images for reference. As severity of cases increases, there is a visible reduction in emerin expression at the nuclear envelope and more deformed nuclei are present. (B) Quantification of emerin staining on IHC-stained patient samples using 0-3, with 0 having no staining at the nuclear periphery and 3 having complete, dark rim staining. N=183 total samples, *P<0.05, **P<0.0001, one-way ANOVA and Dunnett's test. Error bars represent standard deviation.

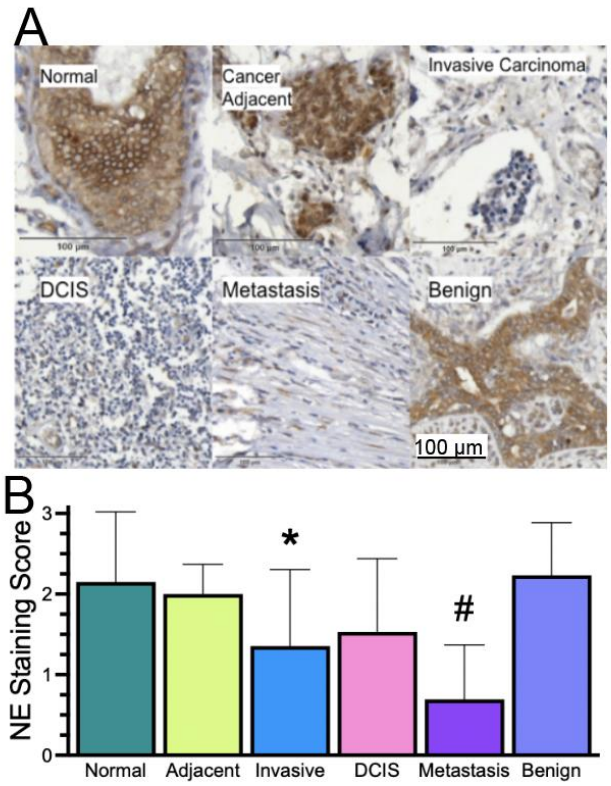

Figure 10

Figure 10: Reduced emerin staining at the nuclear periphery in invasive breast cancer patient samples is confirmed with a monoclonal emerin antibody. A) Representative tissue microarray staining of emerin in 183 patients using emerin monoclonal antibodies (Leica, NCL-Emerin) using the same samples in Figure 9. Nuclei are blue and emerin is brown. As severity of case increases, there is a visible reduction in emerin expression and more deformed nuclei are present. (B) Quantification of emerin staining using the same grading system as in Figure 9. N=183 total samples #P<0.02 compared to all non-cancerous tissue, *P<0.0062 compared to both normal and benign tissue, one-way ANOVA and Dunnett's test. Error bars represent standard deviation.

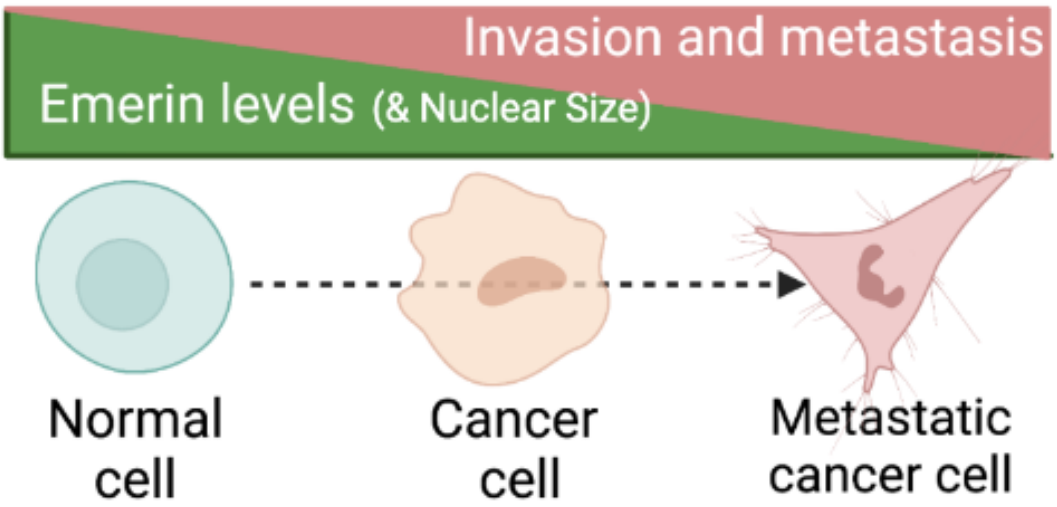

Figure 11

Figure 11: Graphical summary showing how emerin levels impact cancer progression.

Supplemental Figures

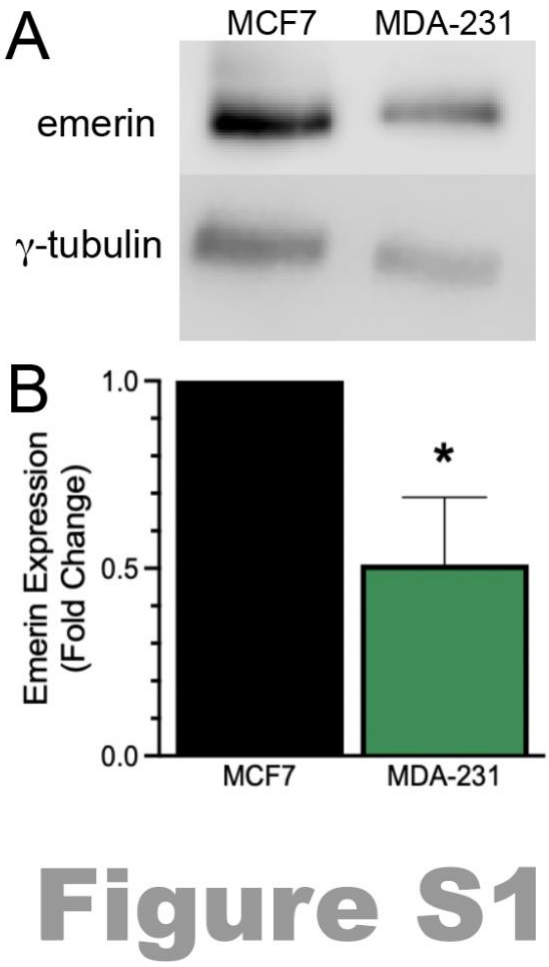

Figure S1

Figure S1: Relative emerin levels in poorly invasive MCF7 and highly invasive MDA-231 cells. A) Representative western blot and B) quantification of emerin protein in MCF7 and MDA-231 cell lines normalized to γ-tubulin. MDA-231 cells have 49% less emerin expression than poorly invasive MCF7 cells; N=4. *P=0.0342, student's t-test. Error bars represent standard error of the mean.

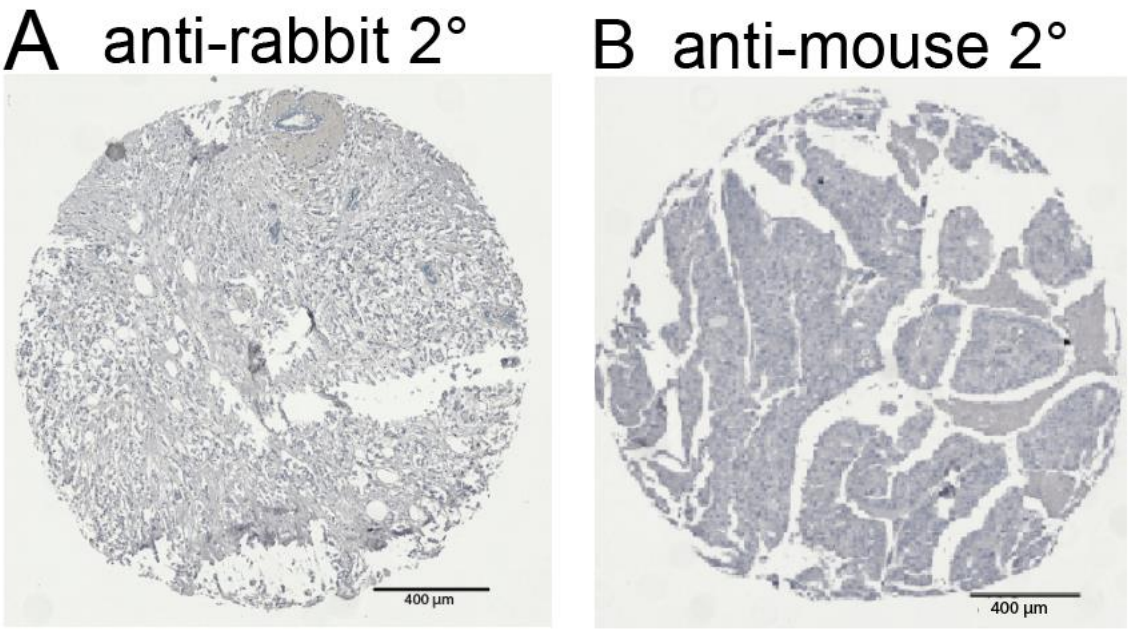

Figure S2

Figure S2: Secondary antibodies incubated alone in tissue microarrays. A) Background staining of anti-rabbit secondary (Vector Lab, cat#: MP-7451) from figure 9 and B) background staining of anti-mouse secondary (Vector Lab, cat# MP-7452) from figure 10. This demonstrates the specificity of emerin staining measured in figures 9 and 10.

References

1. Bussolati G, Marchio C, Gaetano L, Lupo R, Sapino A. Pleomorphism of the nuclear envelope in breast cancer: a new approach to an old problem. J Cell Mol Med.

2008;12(1):209-18. Epub 20071205. doi: 10.1111/j.1582-4934.2007.00176.x. PubMed PMID: 18053086; PMCID: PMC3823482.

2. Acerbi I, Cassereau L, Dean I, Shi Q, Au A, Park C, Chen YY, Liphardt J, Hwang ES, Weaver VM. Human breast cancer invasion and aggression correlates with ECM stiffening and immune cell infiltration. Integr Biol (Camb). 2015;7(10):1120-34. Epub 20150511. doi: 10.1039/c5ib00040h. PubMed PMID: 25959051; PMCID: PMC4593730.

3. Kokai E, Beck H, Weissbach J, Arnold F, Sinske D, Sebert U, Gaiselmann G, Schmidt V, Walther P, Munch J, Posern G, Knoll B. Analysis of nuclear actin by overexpression of wild-type and actin mutant proteins. Histochem Cell Biol. 2014;141(2):123-35. Epub 20131004. doi: 10.1007/s00418-013-1151-4. PubMed PMID: 24091797.

4. Kai F, Laklai H, Weaver VM. Force Matters: Biomechanical Regulation of Cell Invasion and Migration in Disease. Trends Cell Biol. 2016;26(7):486-97. Epub 20160404. doi: 10.1016/j.tcb.2016.03.007. PubMed PMID: 27056543; PMCID: PMC4970516.

5. Hanahan D, Weinberg RA. Hallmarks of cancer: the next generation. Cell. 2011;144(5):646-74. doi: 10.1016/j.cell.2011.02.013. PubMed PMID: 21376230.

6. Hanahan D. Hallmarks of Cancer: New Dimensions. Cancer Discov. 2022;12(1):31-46. doi: 10.1158/2159-8290.CD-21-1059. PubMed PMID: 35022204.

7. Chaffer CL, Weinberg RA. A perspective on cancer cell metastasis. Science. 2011;331(6024):1559-64. doi: 10.1126/science.1203543. PubMed PMID: 21436443.

8. Wirtz D, Konstantopoulos K, Searson PC. The physics of cancer: the role of physical interactions and mechanical forces in metastasis. Nat Rev Cancer. 2011;11(7):512-22. Epub 20110624. doi: 10.1038/nrc3080. PubMed PMID: 21701513; PMCID: PMC3262453.

9. Hansen E, Holaska JM. The nuclear envelope and metastasis. Oncotarget. 2023;14:317-20. Epub 20230414. doi: 10.18632/oncotarget.28375. PubMed PMID: 37057891; PMCID: PMC10103595.

10. Liddane AG, Holaska JM. The Role of Emerin in Cancer Progression and Metastasis. Int J Mol Sci. 2021;22(20). Epub 20211019. doi: 10.3390/ijms222011289. PubMed PMID: 34681951; PMCID: PMC8537873.

11. Liddane AG, McNamara CA, Campbell MC, Mercier I, Holaska JM. Defects in Emerin-Nucleoskeleton Binding Disrupt Nuclear Structure and Promote Breast Cancer Cell Motility and Metastasis. Mol Cancer Res. 2021;19(7):1196-207. Epub 20210326. doi: 10.1158/1541-7786.MCR-20-0413. PubMed PMID: 33771882; PMCID: PMC8254762.

12. Reis-Sobreiro M, Chen JF, Novitskaya T, You S, Morley S, Steadman K, Gill NK, Eskaros A, Rotinen M, Chu CY, Chung LWK, Tanaka H, Yang W, Knudsen BS, Tseng HR, Rowat AC, Posadas EM, Zijlstra A, Di Vizio D, Freeman MR. Emerin Deregulation Links Nuclear Shape Instability to Metastatic Potential. Cancer Res. 2018;78(21):6086-97. Epub 20180828. doi: 10.1158/0008-5472.CAN-18-0608. PubMed PMID: 30154147.

13. Machado S, Mercier V, Chiaruttini N. LimeSeg: a coarse-grained lipid membrane simulation for 3D image segmentation. BMC Bioinformatics. 2019;20(1):2. Epub 20190103. doi: 10.1186/s12859-018-2471-0. PubMed PMID: 30606118; PMCID: PMC6318983.

14. Sutherland RL, Hall RE, Taylor IW. Cell proliferation kinetics of MCF-7 human mammary carcinoma cells in culture and effects of tamoxifen on exponentially growing and plateau-phase cells. Cancer Res. 1983;43(9):3998-4006. PubMed PMID: 6871841.
15. Cos S, Recio J, Sanchez-Barcelo EJ. Modulation of the length of the cell cycle time of MCF-7 human breast cancer cells by melatonin. Life Sci. 1996;58(9):811-6. doi: 10.1016/0024-3205(95)02359-3. PubMed PMID: 8632728.
16. Chow KH, Factor RE, Ullman KS. The nuclear envelope environment and its cancer connections. Nat Rev Cancer. 2012;12(3):196-209. Epub 20120216. doi: 10.1038/nrc3219. PubMed PMID: 22337151; PMCID: PMC4338998.
17. van Diest PJ, van der Wall E, Baak JP. Prognostic value of proliferation in invasive breast cancer: a review. J Clin Pathol. 2004;57(7):675-81. doi: 10.1136/jcp.2003.010777. PubMed PMID: 15220356; PMCID: PMC1770351.
18. Lavenus SB, Vosatka KW, Caruso AP, Ullo MF, Khan A, Logue JS. Emerin regulation of nuclear stiffness is required for fast amoeboid migration in confined environments. J Cell Sci. 2022;135(8). Epub 20220503. doi: 10.1242/jcs.259493. PubMed PMID: 35362531.
19. Guck J, Schinkinger S, Lincoln B, Wottawah F, Ebert S, Romeyke M, Lenz D, Erickson HM, Ananthakrishnan R, Mitchell D, Kas J, Ulvick S, Bilby C. Optical deformability as an inherent cell marker for testing malignant transformation and metastatic competence. Biophys J. 2005;88(5):3689-98. Epub 20050218. doi: 10.1529/biophysj.104.045476. PubMed PMID: 15722433; PMCID: PMC1305515.
20. Suresh S. Nanomedicine: elastic clues in cancer detection. Nat Nanotechnol. 2007;2(12):748-9. Epub 20071202. doi: 10.1038/nnano.2007.397. PubMed PMID: 18654425.
21. Denis KB, Cabe JI, Danielsson BE, Tieu KV, Mayer CR, Conway DE. The LINC complex is required for endothelial cell adhesion and adaptation to shear stress and cyclic stretch. Mol Biol Cell. 2021;32(18):1654-63. Epub 20210630. doi: 10.1091/mbc.E20-11-0698. PubMed PMID: 34191529; PMCID: PMC8684736.
22. Lombardi ML, Jaalouk DE, Shanahan CM, Burke B, Roux KJ, Lammerding J. The interaction between nesprins and sun proteins at the nuclear envelope is critical for force transmission between the nucleus and cytoskeleton. J Biol Chem. 2011;286(30):26743-53. Epub 20110607. doi: 10.1074/jbc.M111.233700. PubMed PMID: 21652697; PMCID: PMC3143636.
23. Capo-chichi CD, Cai KQ, Simpkins F, Ganjei-Azar P, Godwin AK, Xu XX. Nuclear envelope structural defects cause chromosomal numerical instability and aneuploidy in ovarian cancer. BMC Med. 2011;9:28. Epub 20110326. doi: 10.1186/1741-7015-9-28. PubMed PMID: 21439080; PMCID: PMC3072346.
24. Lammerding J, Hsiao J, Schulze PC, Kozlov S, Stewart CL, Lee RT. Abnormal nuclear shape and impaired mechanotransduction in emerin-deficient cells. J Cell Biol. 2005;170(5):781-91. Epub 20050822. doi: 10.1083/jcb.200502148. PubMed PMID: 16115958; PMCID: PMC2171355.